Changes to Peroxyacyl Nitrates (PANs) over Megacities in Response to COVID-19 Tropospheric NO_2 Reductions Observed by the Cross-track Infrared Sounder (CrIS)

Madison J. Shogrin[1], Vivienne H. Payne[2], Susan S. Kulawik[3], Kazuyuki Miyazaki[2], and Emily V. Fischer[1]

[1]Colorado State Univerity, Department of Atmospheric Science, Fort Collins, CO, USA.
[2]Jet Propulsion Laboratory, California Institute of Technology, Pasadena CA, USA.
[3]Bay Area Environmental Research Institute, Petaluma, CA, USA.

Corresponding author: Madison J. Shogrin (madison.shogrin@colostate.edu)

Key Points:

- There are pronounced seasonal cycles of PANs over each megacity that align with seasonal maximums in photochemistry.
- Observed free tropospheric mixing ratios of PANs during COVID-19 were significantly different over two out of eight surveyed megacities.
- Sensitivity of free tropospheric PANs to the abundance of precursors is seasonally dependent in some locations.

Abstract

The COVID-19 pandemic perturbed air pollutant emissions as cities shutdown worldwide. Peroxyacyl nitrates (PANs) are important tracers of photochemistry that are formed through the oxidation of non-methane volatile organic compounds (NMVOCs) in the presence of nitrogen oxide radicals (NO_x = NO + NO_2). We use satellite measurements of free tropospheric PANs from the S-NPP Cross-Track Infrared Sounder (CrIS) over eight of the world's megacities: Mexico City, Beijing, Los Angeles, Tokyo, São Paulo, Delhi, Lagos, and Karachi. We quantify the seasonal cycle of PANs over these megacities and find seasonal maxima in PANs correspond to seasonal peaks in local photochemistry. CrIS is used to explore changes in PANs in response to the COVID-19 lockdowns. Statistically significant changes to PANs occurred over two megacities: Los Angeles (PAN decreased) and Beijing (PAN increased). Our analysis suggests that large perturbations in NO_x may not result in significant declines in NO_x export potential of megacities.

Plain Language Summary

The COVID-19 pandemic led to the lockdown of urban centers worldwide, drastically perturbing the concentrations of global air pollutants. Peroxyacyl nitrates (PANs) are important photochemical pollutants formed from reactions between NO_x and volatile organic compounds (VOCs), which were substantially reduced during the pandemic. We use satellite measurements of PANs from the Suomi-National Polar-orbiting Partnership (S-NPP) Cross-Track Infrared Sounder (CrIS) in the free troposphere over and surrounding eight of the world's megacities: Mexico City, Beijing, Los Angeles, Tokyo, São Paulo, Delhi, Lagos, and Karachi. Seasonal cycles of PANs are pronounced and the seasonal maxima correspond to seasonal peaks in local photochemistry. Significant changes to PANs in response to COVID-19 occurred over two out of the eight cities: Los Angeles (PANs decreased) and Beijing (PANs increased). Our results indicate that large changes in NO_x may not result in equally significant changes to PANs and the NO_x export potential of megacities.

1 Introduction

To slow the spread of the 2019 novel coronavirus (COVID-19), urban centers across the globe partially shut down for various amounts of time (Chinazzi et al., 2020; WHO, 2020). While the timing differed for each urban region, a consequence of these bursts of reduced economic activity was a radical decrease in the emissions of many primary air pollutants. Reductions in global and regional particulate matter, nitrogen oxides (NO_x = NO + NO_2), carbon dioxide (CO_2), and other trace gasses associated with the COVID-19 pandemic have been documented (Bauwens et al., 2020; Z. Liu et al., n.d.; Miyazaki, Bowman, Sekiya, Jiang, et al., 2020; Miyazaki et al., 2021; Odekanle et al., 2022; Sharma et al., 2020; Shi & Brasseur, 2020; Venter et al., 2020; J. Zhang et al., 2022) Less is understood about changes to secondary pollutants as they respond non-linearly to changes in precursor emissions, and their production and lifetime also depend on environmental conditions (*e.g.*, Stavrakou et al., 2021). For example, both increases and decreases in surface ozone (O_3) have been documented in urban areas during the COVID-19 pandemic despite decreases in precursor emissions (*e.g.,* Le et al., 2020; Miyazaki et al., 2021; Qiu et al., 2020; Shi & Brasseur, 2020; Sicard et al., 2020).

Peroxyacyl nitrates (PANs) are important photochemically-produced species that are formed alongside O_3 in polluted environments by the oxidation of non-methane volatile organic compounds (NMVOCs) in the presence of NO_x (Fischer et al., 2014; Gaffney et al., 1989; Roberts, 2007; Singh et al., 1986; Singh & Hanst, 1981). PANs are considered to be a sensitive tracer of photochemistry (e.g., Coggon et al., 2021; Rappenglück et al., 2003). Formation and decomposition of PANs can impact the production of O_3 (e.g. Steiner et al., 2010), the production of PANs acts as an indicator of regional photochemistry (Sillman & West, 2009), and the concentration of PANs can be used to gauge effectiveness of O_3-control strategies (Gaffney et al., 1989). PANs respond to precursor emissions non-linearly and have been shown to be more sensitive to changes in NMVOCs versus changes in NO_x for

many regions of the global atmosphere (Fischer et al., 2014) and in some urban regions (T. Liu et al., 2022).

The lifetime of PANs against thermal decomposition is strongly dependent on temperature, where PANs are thermally unstable in the lower troposphere (lifetime on the order of hours at 20°C), but have a lifetime >1 month at temperatures characteristic of the mid-troposphere (Honrath et al., 1996). When transported from polluted continental regions to the remote troposphere, PANs serve as the principal reservoir species for NO_x and can contribute to efficient production of downwind O_3 in NO_x limited conditions (Fischer et al., 2014; Mena-Carrasco et al., 2009). The distribution of O_3 in the remote atmosphere would be substantially different without PAN chemistry (e.g., Jiang et al., 2016). There have been major changes in NO_x and VOC emissions in urban areas in recent decades, elevating the need for continued and extended observations of photochemically-relevant species in urban regions. In situ measurements of PANs have been collected for select urban areas for select seasons (Gaffney et al., 1989; Qiu et al., 2019; G. Zhang et al., 2015a), though observations are generally sparse.

Here we present new satellite observations of PANs over eight megacities. We utilize measurements from the Suomi-National Polar-orbiting Partnership (S-NPP) Cross-Track Infrared Sounder (CrIS) and other complimentary satellite and reanalysis datasets to document the seasonal cycles of PANs over select megacities and the response of PANs to COVID-19 induced reductions of precursor concentrations in these locations.

2 Materials and Methods

2.1 CrIS Observations

We use observations of free tropospheric PANs and CO from the CrIS instrument, a nadir viewing Fourier transform spectroradiometer currently flying on the S-NPP satellite. The datasets used here were produced under the NASA Tropospheric Ozone and Precursors from Earth System Sounding (TROPESS) project (Bowman, 2021c, 2021k, 2021o, 2021a, 2021e, 2021i, 2021l, 2021p, 2021d, 2021j, 2021b, 2021f, 2021c; Shogrin, 2023). Information on the CrIS PANs retrieval algorithm and validation against aircraft observations can be found in Payne et al. (2022). The validation efforts for the CrIS PANs product suggest a single sounding uncertainty of around 0.08 ppbv that reduces with averaging to an approximate floor of 0.05 ppbv and demonstrates the ability of CrIS to capture variation in the "background" PANs over remote regions (Payne et al., 2022). The CrIS CO algorithm is described in Fu et al. (2016) and validation is presented in Worden et al. (2022). A single sounding uncertainty for CrIS CO retrievals is on the order of 6-10% (Worden et al., 2022) and this is expected to reduce with averaging. Our analysis uses the column average PANs volume mixing ratio (VMR) between 825 and 215 hPa. CrIS PANs retrievals have peak sensitivity in the free troposphere (~680 hPa) and the sensitivity decreases rapidly near the surface. At most, CrIS PANs retrievals have 1 degree of freedom for signal (DOF), meaning this product does not include information about the vertical distribution of PANs in the atmosphere. The spectral feature utilized by CrIS for retrieval of PANs is centered at 790 cm^{-1}. This infrared spectral feature appears in the spectra of all PANs at essentially the same frequency, so CrIS measurements include all PAN species (i.e., they include propionyl peroxy nitrate (PPN; $CH_3CH_2C(O)OONO_2$), methacryloyl peroxy nitrate (MPAN; $CH_2C(CH_3)C(O)OONO_2$), etc.) in addition to peroxyacetyl nitrate (PAN; $CH_3C(O)O_2NO_2$). We also use a tropospheric average of CrIS CO between 825 hPa and 215 hPa. Our analysis focuses on CrIS PANs over and around 9 megacities utilizing CrIS CO to contextualize seasonal enhancements in PANs.

PAN observations from nadir-viewing satellites include those from the Tropospheric Emission Spectrometer (TES) (Payne et al., 2014) as well as meteorological sounders namely the Infrared Atmospheric Sounding Interferometer (IASI) (Franco et al., 2018) and CrIS (Payne et al., 2022). Studies observing PAN from space thus far have focused on PAN enhancements associated with fires (Alvarado

et al., 2011; Clarisse et al., 2011; Juncosa Calahorrano et al., 2021) and the global distribution of PAN and its role in the long range transport of O_3 (Fischer et al., 2018; Jiang et al., 2016; Payne et al., 2017; Zhu et al., 2015; 2017). Although TES had provided a set of special observations over select megacities (Cady-Pereira et al., 2017; Shogrin et al., 2023), the spatial and temporal coverage of this dataset is somewhat limited. Here, we utilize the more comprehensive spatial and temporal coverage of CrIS to explore the spatiotemporal distribution of PANs over and around megacities.

2.2 Ozone Monitoring Instrument (OMI) Observations

We use Level 3 NO_2 tropospheric column measurements from NASA Aura-OMI to identify months with anomalously low NO_2 columns associated with COVID in 2020. We use the Quality Assurance for Essential Climate Variables (QA4ECV) NO_2 Level 3 product described in Boersma et al. (2018) as this is the most recently updated data product. OMI NO_2 L3 monthly mean data used in this study is provided on a global 0.125° x 0.125° grid and can be found on the TEMIS database (Boersma et al., 2017b).

We use Level 3 (L3) HCHO tropospheric column measurements, also from OMI, to contextualize changes in monthly VOC concentrations in megacities during the period of anomalously low tropospheric NO_2. Space-based observations of HCHO are used as an indicator of VOC emissions (De Smedt et al., 2008; Shen et al., 2019). HCHO is also processed using the QA4ECV algorithm consistently with the NO_2 data used in this study. HCHO L3 monthly mean data is also provided on a global 0.125° x 0.125° grid and can also be found on the TEMIS database (De Smedt et al., 2017).

2.3 Chemical Reanalysis Product

We use NO_x emission reanalysis data to also place changes to PANs in the context of NO_x emission flux reductions in megacities associated with COVID-19. NO_x emissions are from an assimilation of multi-species satellite observations (O_3, CO, NO_2, HNO_3, and SO_2) in the Tropospheric Chemistry Reanalysis version 2 (TCR-2) framework (Miyazaki et al., 2020; https://doi.org/10.25966/9qgv-fe81). NO_x emissions are constrained by tropospheric column NO_2 retrievals from the QA4ECV version 1.1 Level 2 products from OMI and Global Ozone Monitoring Experiment 2 (GOME-2) (Boersma et al., 2017a, 2017b). A priori emissions are from HTAP version 2 for 2010 (Janssens-Maenhout et al., 2015), Global Fire Emissions Database (GFED) version 4 (Randerson et al., 2018), and the Global Emissions Inventory Activity (GEIA) (Graedel et al., 1993). The reanalysis fields have been evaluated against independent observations on regional and global scales (Miyazaki et al., 2020). NO_x emissions for 2020 used in our analysis are estimated using business as usual (BAU) emissions added to the estimated COVID-19 emissions anomaly described in Miyazaki et al. (2021). While the observed NO_2 concentrations are affected by meteorological concentrations, their effect is already taken into account when estimating the NO_x emissions (Miyazaki et al., 2017; 2020)

3 Results and discussion

3.1 Seasonal Cycles of PANs, CO, and HCHO in megacities

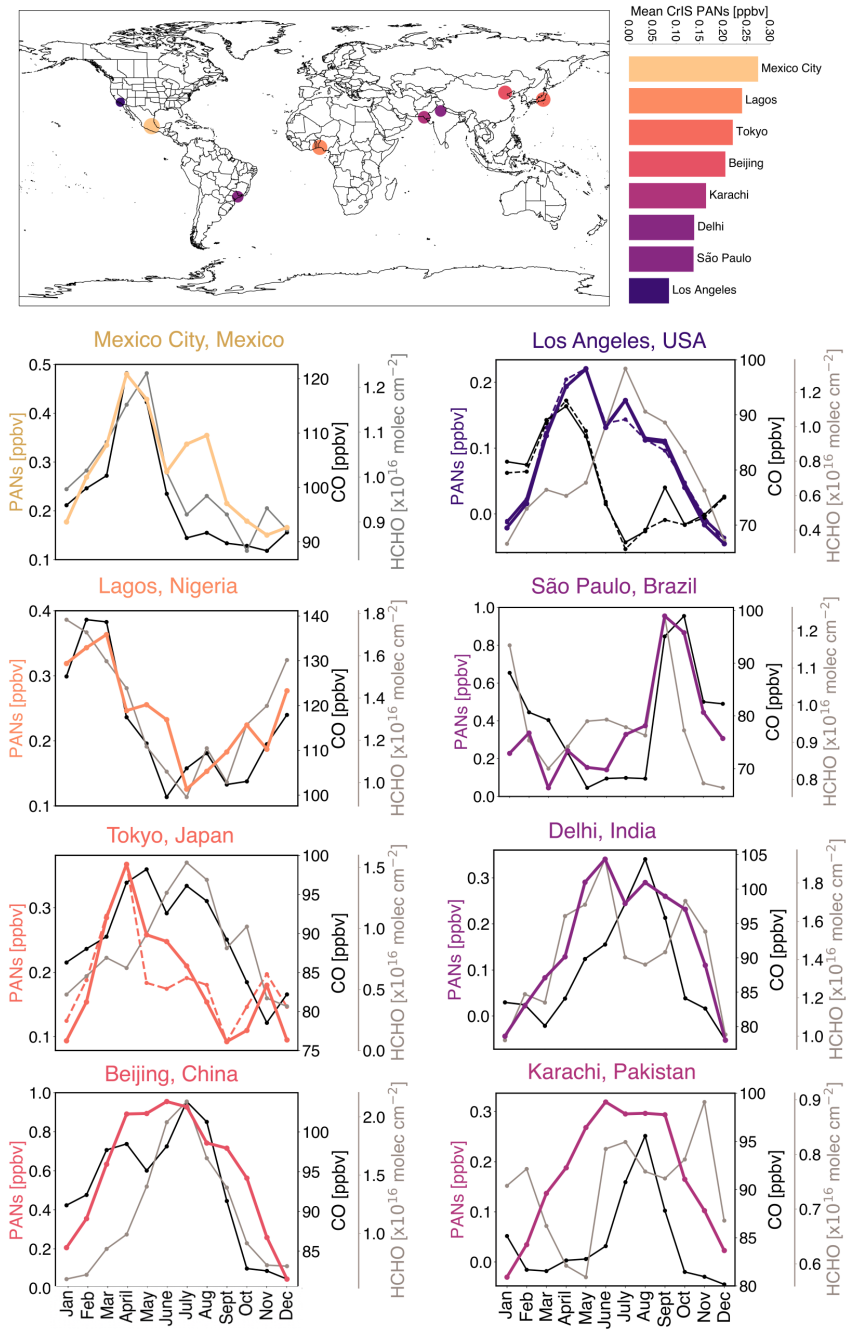

Figure 1. Top: Map shows mean detected CrIS PANs for the entire study period. The scale to the right of the map ranks the cities using the mean PANs. Dot sizing is indicative of abundance of mean PANs. Seasonal cycles of CrIS PANs [ppbv] (color denoted in color bar, dashed denotes median values), CrIS tropospheric CO [ppbv] (dark grey), and OMI HCHO tropospheric column average [x10^{16} molecules cm^{-2}]

(lighter grey) for eight megacities. Note: scales vary for each plot. Monthly means include data from January 2016 to May 2021.

Figure 1 displays the mean seasonal cycles for CrIS PANs, CrIS CO, and OMI HCHO for eight different global megacities from 2016-2021. Figure 1 helps identify periods in the annual cycle with production of PANs and values of PANs above a threshold where CrIS is able to provide quantitative information. For most cities, NO_2 changes from COVID-19 coincide with periods where PANs are above the CrIS detection limit (Section 2.1) and conditions support photochemical production.

All but two selected megacities experience a springtime maxima in PANs. The seasonal springtime maximum in PANs is attributed to an increase in photochemical activity at a time when PANs have a relatively long lifetime against thermal decomposition (Brice et al., 1988; Fischer et al., 2014; Penkett & Brice, 1986). Seasonal maxima occur in March, April, and/or May for northern hemisphere megacities (Mexico City, Los Angeles (LA), Tokyo, Delhi, and Lagos), and in September for São Paulo (23.56°S), the beginning of austral spring. Over Lagos (6.52°N) PANs begin increasing towards the end of the calendar year and maximize in March or April. In addition to a springtime maxima, PANs over Beijing (39.92°N) and Karachi (24.86°N) remain elevated through the summer (April-September). Though it has a springtime maxima, Delhi (28.71°N) has a comparably wide seasonal cycle in PANs. Mexico City, LA, and Tokyo also show an additional period of elevated PANs later in the year.

PANs over each megacity reflect a combination of sources and meteorological conditions, but the extent of the published literature on air pollutants in each megacity differs widely. Here we focus our discussion on LA, Beijing, and to a more limited extent, Tokyo, Delhi, and Lagos.

There is a longstanding effort to attribute and control O_3 and other photochemical pollutants in LA (Langford et al., 2010; Nussbaumer & Cohen, 2020; Pollack et al., 2013; Warneke et al., 2013). CrIS data indicate that the seasonal cycle in PANs over LA is distinct from both HCHO and surface O_3 (not shown); tropospheric column HCHO and surface O_3 have broad maxima extending from April through October and June through October, respectively. Increasing temperatures during the summer decrease the lifetime of PANs due to thermal decomposition and decrease the ratio of free tropospheric PANs to surface O_3. The secondary and tertiary peaks in monthly mean PANs over LA in July and September are driven by wildfire smoke transported into the LA Basin in 2018 and 2020, respectively (Liang et al., 2021). Wildfire impacts in September 2020 also drive the peak in September CO; note the difference between the mean and median as these peaks are not evident in the median (dashed) CO and PANs for these months.

Information on PANs within and around Beijing is growing rapidly (e.g., Z. Liu et al., 2010; B. Zhang et al., 2017, 2019). In Beijing, surface O_3 and tropospheric column HCHO have seasonal maxima in summer months (JJA), corresponding to the seasonal maximum in CrIS PANs (Figure 1) and recorded surface observations of PAN and PPN (B. Zhang et al., 2017; G. Zhang et al., 2015b). Ground-level PAN is also elevated during winter haze events in Beijing (Li et al., 2021; Qiu et al., 2019; B. Zhang et al., 2019; G. Zhang et al., 2020). CrIS observes elevated CO over Beijing in March and April, consistent with a seasonal peak in local fire activity in northeast China (Feng et al., 2015; L. Wang et al., 2020; Yin et al., 2019; Zhao et al., 2022).

Tokyo has a seasonal spring maximum in photochemical species from both local and distant (*i.e.,* China and Korea) sources of precursors (Lee et al., 2021; Yoshitomi et al., 2011). Delhi has a humid subtropical/semi-arid climate and air pollution is strongly influenced by the Indian monsoon (Gurjar et al., 2016). The monsoon season lasts from July-September and the dry season is considered to be September-June. CrIS observes elevated PANs over Delhi from April to October; on average PANs remain elevated through the monsoon season. Crop residue burning in April-May and October-November can deteriorate air quality in the Delhi metropolitan area (Saxena et al., 2021). These periods correspond with periods of elevated PANs and tropospheric column HCHO. Lagos surface O_3 increases seasonally during the dry season (Abdul Raheem et al., 2009). This is consistent with CrIS observations of PANs and CO, which increase and decrease with the respective dry and wet seasons.

3.2 2020 NO_2 Anomalies

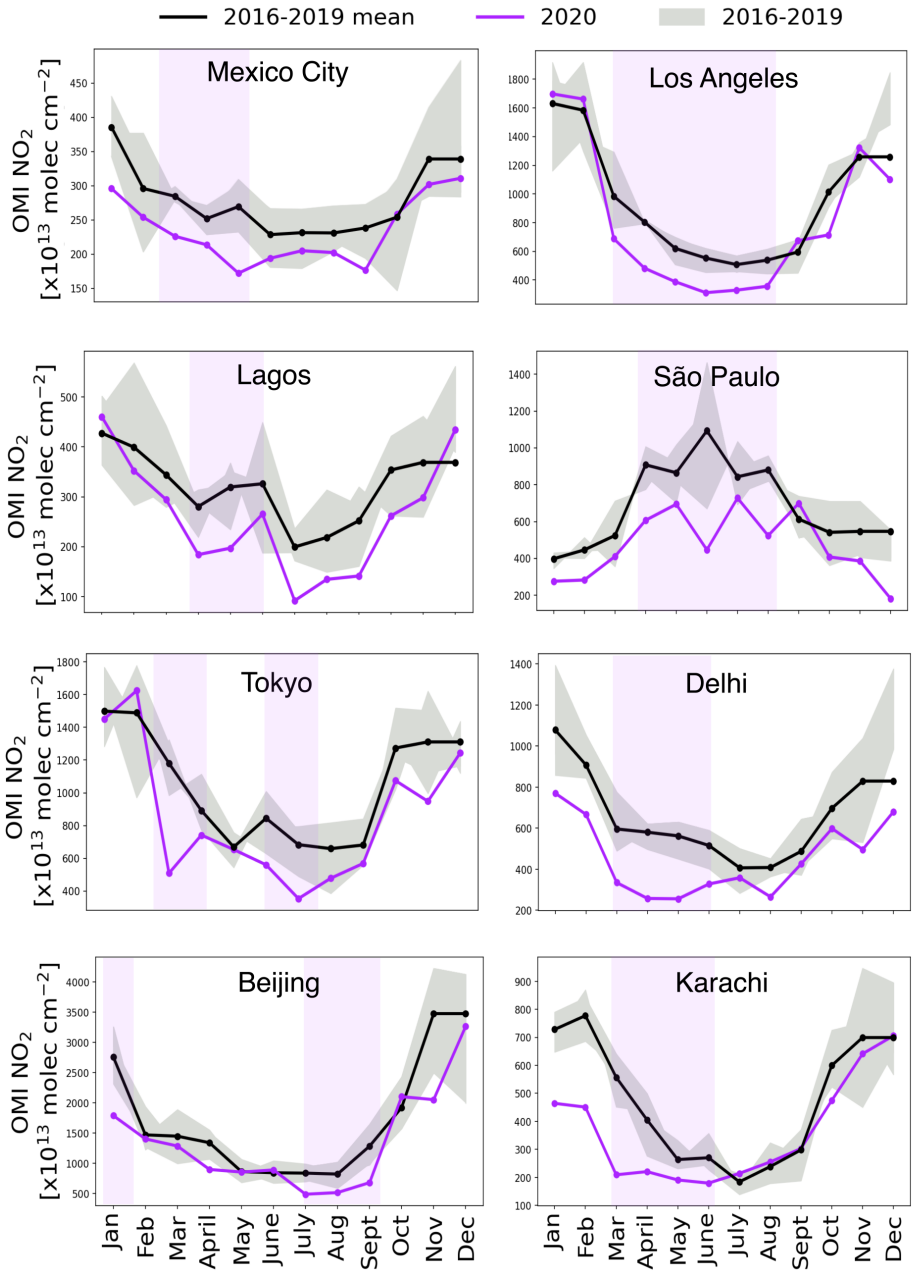

Figure 2. OMI NO_2 tropospheric column monthly means for 9 megacities. The area used for each city is the same area around the urban area of each city used for CrIS selection and this information is provided in Table 1. 2020 is shown in purple. The mean of 2016-2019 is shown in bold black. Months with substantial NO_2 declines in 2020 have been highlighted in purple shading and these time frames are used in the subsequent analysis presented in Figure 3.

Major changes in NO_x emissions and tropospheric NO_2 column abundances have been documented worldwide for different periods of the COVID-19 pandemic (Bauwens et al., 2020; Berman & Ebisu,

2020; J. Zhang et al., 2022). For the analysis presented here, we identify periods where 1) the monthly mean NO_2 column during 2020 was at least 15% below the corresponding monthly mean for 2016-2019 (black line in Figure 2), and 2) the monthly mean PANs mixing ratio are at least 0.05 ppbv (Figure 1). We only consider times in the seasonal cycle where mixing ratios of PANs are at least 0.05 ppbv because this corresponds with the uncertainty discussed in Section 2.1 and Payne et al. (2022). The months that meet these criteria are highlighted by the light purple shading in Figure 2. The 2020 monthly mean NO_2 column density associated with these shaded periods is at least 15% less than the mean of the corresponding months for the period 2016-2019. Periods of lower observed NO_2 often do not exactly coincide with the COVID-19 government-enforced lockdowns, as reduced traffic was often observed prior to government-imposed stay-at-home orders.

Table 1. Changes to Chemical Species during Respective Time Periods.

City	Monthly mean time period	NO2 change (%)	NOx change (%)	HCHO change (%)	PANs change (%)	P-value
Mexico City	February-May	-22%	-14%	5.6%	1.8%	0.45
Beijing	January	-35%	-19%	59%	80%	0.03
Beijing	July-September	-40%	-16%	-7.6%	-1.9%	0.31
Tokyo	March-April	-40%	-23%	-26%	6.9%	0.11
Tokyo	June-July	-40%	-15%	-43%	-0.9%	0.44
Los Angeles	March-August	-36%	-17%	-10%	-11%	0.06
São Paulo	April-August	-35%	-11%	-1.7%	3.7%	0.33
Delhi	March-June	-48%	-28%	-9.6%	-20%	0.33
Lagos	April-June	-35%	-16%	-0.08%	11%	0.33
Karachi	March-June	-52%	-5%	3.6%	12%	0.14

Table 1. Periods of significant NO_2 decline based on tropospheric column OMI NO_2 monthly means shown in Figure 2. Percent change represents the change in 2020 values relative to the mean of 2016-2019 for the respective time periods. Percent change in PANs were calculated using daily means during the months of NO_2 anomaly. P-values are from Mann-Whitney u test. A negative percent change signifies a decline in 2020 relative to the same months in prior years; likewise, positive percent changes signify an increase.

3.3 Impacts of COVID-19 NO_x reductions on PANs over megacities

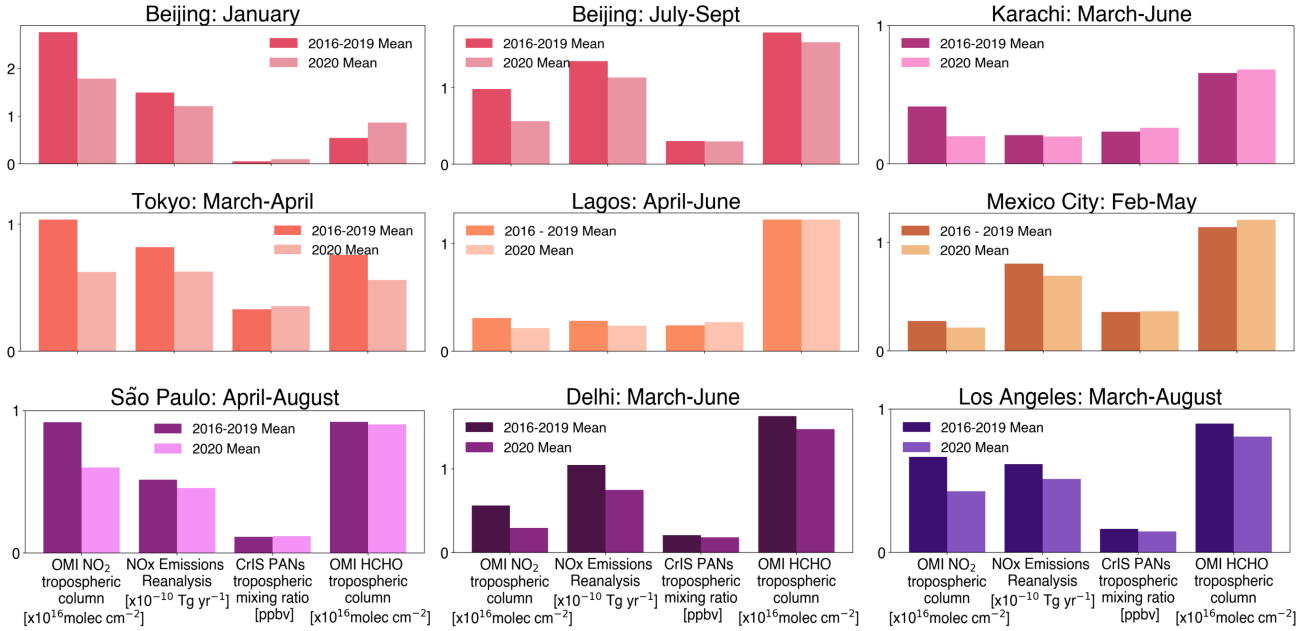

Figure 3. Bar charts comparing monthly means for specified months of OMI NO_2 tropospheric columns [x10^{16} molecules cm^{-2}], NO_x emissions from the Tropospheric Chemical Reanalysis [x10^{-10} Tg yr^{-1}], CrIS free troposphere PANs [ppbv], and OMI HCHO tropospheric columns [x10^{16} molecules cm^{-2}] for each megacity. Means of monthly means for specified periods in 2020 (shown in Figure 2 and listed in Table 1) are plotted in the lighter colors and means of 2016-2019 are plotted in the darker colors. We performed a Mann-Whitney u-test to test the significance of changes to PANs during the respective time periods of COVID-19 NO_2 perturbations listed in Table 1; 2020 was compared to the same time period from 2016-2019. We set our alpha at 0.1, so p values < 0.1 are considered significant and receive more discussion.

Figure 3 shows that while there were large decreases in NO_2 declines at some point in 2020, this did not yield a similarly large change in free tropospheric PANs for each region. Most megacities surveyed did not experience significant change in PANs at the 90% confidence level, except for LA, which experienced a significant decline, and Beijing in winter, which experienced a significant increase. We expect that PANs (and the sensitivity of CrIS) would also respond to other environmental factors including temperature; we analyze two possible environmental indicators: 2 meter air temperature and 500 hPa air temperature changes between the two respective periods over each of the megacities using MERRA-2 Reanalysis monthly mean product (Global Modeling and Assimilation Office (GMAO), 2015; DOI:10.5067/AP1B0BA5PD2K). We find no significant change in mean temperature at either pressure level between 2020 and corresponding months during the prior 4 years. Thus temperature was likely not a significant factor driving anomalies in PANs during the extended periods of NO_x perturbations highlighted in Figure 2. PANs have been used to gauge effectiveness of O_3-control strategies (*e.g.*, Gaffney et al., 1989). The tropospheric column ratios of HCHO to NO_2 have been used as a qualitative indicator of NO_x sensitive versus NO_x saturated (VOC-limited) regimes (*e.g.,* Jin et al., 2017; Martin et al., 2004; Souri et al., 2023). Threshold values vary by location (Souri et al., 2020), but higher (lower) ratios indicate NO_x-sensitive (saturated) conditions. Reductions in NO_x during the pandemic were substantial enough to shift the photochemical regime in some areas, *i.e.,* from NO_x-saturated to a transition zone or from a transition zone to NO_x-sensitive conditions (Peralta et al., 2021). The SI contains a version of Table 1 that also includes tropospheric column HCHO:NO_2 ratios over each city. We did not

identify a consistent relationship between this ratio and the sensitivity of PAN to COVID induced-changes to NO_x.

PANs decreased significantly over LA during COVID-19 NO_x emission reductions, and this coincided with decreases in surface O_3 (Connerton et al., 2020; Schroeder et al., 2022). The underlying photochemical environment of LA has been transitioning from a VOC-limited regime to a NO_x-limited regime (Lee et al., 2021; Schroeder et al., 2022); spring 2020 was the first NO_x-limited year (Schroeder et al., 2022). PAN abundances at the ground have decreased much more rapidly than O_3 in response to emission controls in the LA Basin (Pollack et al., 2013). The CrIS data suggest that PAN would continue to respond to NO_x emission reductions in this city.

PANs did not show marked changes over Mexico City, São Paulo or Tokyo despite major NO_x perturbations. O_3 over Tokyo also did not significantly change with COVID-19 lockdown measures; this has been attributed to a shift in the underlying photochemical regime from VOC-limited towards the transition zone where O_3 production is expected to be equally sensitive to changes in both NO_x and VOCs (Damiani et al., 2022; Ito et al., 2021; Q. Wang & Li, 2021). O_3 in Mexico City was also statistically indistinguishable during periods of substantial precursor reduction in 2020 from that of other years (Peralta et al., 2021). São Paulo experienced an increase in O_3 in April and May, but largely in areas most seriously impacted by vehicle emissions (Alvim et al., 2023).

The largest and only significant increase in free tropospheric PANs on a monthly mean scale in our analysis occurred over Beijing in January (80%, $p = 0.03$), coincident with the lowest average HCHO: NO_2 ratio of all cities included here. Qiu et al. (2020) reported a threefold increase in ground-level PAN in urban Beijing during this first lockdown period, connected to enhanced local photochemistry and abnormal meteorological conditions, including anomalous wind convergence under higher temperatures. We find a similar change in free tropospheric PANs over Beijing, where mean CrIS PANs are 2.4 times higher during the same lockdown period. Beijing had a second period of NO_2 decline in July and August 2020, which was associated with an insignificant change in PANs (-1.96%, $p = 0.31$). Stavrakou et al. (2021) also investigated the impact of COVID-19 on PAN over China.

5 Conclusions

We use CrIS data from 2016-2021 to identify the seasonality of PANs over 8 megacities, and identify time periods with elevated PANs. This is the first detailed analysis of satellite observations of PANs over multiple megacities. We use this to inform our analysis in diagnosing the impact of NO_2 declines related to the COVID-19 pandemic on PANs in these locations.

1. There are pronounced seasonal cycles in PANs over each megacity. Monthly mean PANs peak in the spring or summer (Beijing and Karachi), aligning with respective seasonal maximums in photochemical activity. Wildfire smoke can occasionally enhance monthly mean PANs.

2. Despite large changes in tropospheric NO_2 columns associated with the COVID-19 pandemic, we only identify two megacities over which PANs changed significantly: Beijing and LA. The relative response of PANs in these locations was smaller than the changes in NO_2. The response of PANs to a major change in precursor emissions is highly non-linear.

3. Sensitivity of free tropospheric PANs to the abundance of precursors appears to be seasonally dependent in Beijing and Tokyo. PANs over Beijing and Tokyo are likely more sensitive to NO_x reductions in winter and spring respectively.

4. Based on this survey of megacities, relatively large perturbations in NO_x may not result in significant declines in NO_x export potential of megacities in all seasons. Thus satellite observations of PANs may be an additional useful diagnostic in predicting the complex response of O_3 to NO_x reductions in downwind regions. Next steps should focus on identifying the response of PAN downwind of megacities to COVID-19 NO_x reductions.

Acknowledgments

This work is funded under NASA award no. 80NSSC20K0947. Part of this work was carried out at the Jet Propulsion Laboratory, California Institute of Technology, under a contract with the National Aeronautics and Space Administration (80NM0018D0004). We thank Isabelle De Smedt and Folkert Boersma for collaborating on the proposal that led to this work and for answering questions regarding the OMI data.

Open Research

The Summary and Standard Product of CrIS PANs megacity Special Collection data for each megacity used in this study are available online through the Goddard Earch Sciences Data and Information services Center (NASA GES DISC) (Bowman, 2021c, 2021k, 2021g, 2021o, 2021a, 2021e, 2021m, 2021i, 2021l, 2021h, 2021p, 2021d, 2021n, 2021j, 2021b, 2021f, 2021c). Megacity datasets for Lagos and São Paulo can be found at https://doi.org/10.5061/dryad.wpzgmsbtk and eventually on the NASA GES DISC. OMI NO_2 and HCHO data were obtained from https://www.temis.nl/airpollution/no2.php and https://h2co.aeronomie.be/ (last access: August 2021), (Boersma et al., 2017b; De Smedt et al., 2017).

References

Abdul Raheem, A. M. O., Adekola, F. A., & Obioh, I. O. (2009). The Seasonal Variation of the Concentrations of Ozone, Sulfur Dioxide, and Nitrogen Oxides in Two Nigerian Cities. *Environmental Modeling & Assessment*, *14*(4), 497–509. https://doi.org/10.1007/s10666-008-9142-x

Alvarado, M. J., Cady-Pereira, K. E., Xiao, Y., Millet, D. B., & Payne, V. H. (2011). Emission Ratios for Ammonia and Formic Acid and Observations of Peroxy Acetyl Nitrate (PAN) and Ethylene in Biomass Burning Smoke as Seen by the Tropospheric Emission Spectrometer (TES). *Atmosphere*, *2*(4), 633–654. https://doi.org/10.3390/atmos2040633

Alvim, D. S., Herdies, D. L., Corrêa, S. M., Basso, L. S., Khalid, B., Silva, G. F. P., Oyerinde, G., De Carvalho, N. A., Coelho, S. M. S. D. C., & Figueroa, S. N. (2023). COVID-19 Pandemic: Impacts on Air Quality during Partial Lockdown in the Metropolitan Area of São Paulo. *Remote Sensing*, *15*(5), 1262. https://doi.org/10.3390/rs15051262

Bauwens, M., Compernolle, S., Stavrakou, T., Müller, J. -F., Gent, J., Eskes, H., Levelt, P. F., A, R., Veefkind, J. P., Vlietinck, J., Yu, H., & Zehner, C. (2020). Impact of Coronavirus Outbreak on NO_2 Pollution Assessed Using TROPOMI and OMI Observations. *Geophysical Research Letters*, *47*(11). https://doi.org/10.1029/2020GL087978

Berman, J. D., & Ebisu, K. (2020). Changes in U.S. air pollution during the COVID-19 pandemic. *Science of The Total Environment*, *739*, 139864. https://doi.org/10.1016/j.scitotenv.2020.139864

Boersma, K. F., Eskes, H. J., Richter, A., De Smedt, I., Lorente, A., Beirle, S., van Geffen, J. H. G. M., Zara, M., Peters, E., Van Roozendael, M., Wagner, T., Maasakkers, J. D., van der A, R. J., Nightingale, J., De Rudder, A., Irie, H., Pinardi, G., Lambert, J.-C., &

Compernolle, S. C. (2018). Improving algorithms and uncertainty estimates for satellite NO₂ retrievals: Results from the quality assurance for the essential climate variables (QA4ECV) project. *Atmospheric Measurement Techniques*, *11*(12), 6651–6678. https://doi.org/10.5194/amt-11-6651-2018

Boersma, K. F., Eskes, H., Richter, A., De Smedt, I., Lorente, A., Beirle, S., van Geffen, J. H. G. M., Peters, E., Van Roozendael, M., & Wagner, T. (2017a). *QA4ECV NO2 tropospheric and stratospheric vertical column data from GOME-2A (Version 1.1) [Data set]*. Royal Netherlands Meteorological Institute (KNMI). http://doi.org/10.21944/qa4ecv-no2-gome2a-v1.1

Boersma, K. F., Eskes, H., Richter, A., De Smedt, I., Lorente, A., Beirle, S., van Geffen, J. H. G. M., Peters, E., Van Roozendael, M., & Wagner, T. (2017b). *QA4ECV NO2 tropospheric and stratospheric vertical column data from OMI (Version 1.1) [Data set]*. Royal Netherlands Meteorological Institute (KNMI). http://doi.org/10.21944/qa4ecv-no2-omi-v1.1

Bowman, K. W. (2021a). *TROPESS CrIS-SNPP L2 Peroxyacetyl Nitrate for Beijing* (Standard Product V1) [dataset]. Goddard Earth Sciences Data and Information Services Center (GES DISC). https://doi.org/10.5067/IUJHNI1MM1QA

Bowman, K. W. (2021b). *TROPESS CrIS-SNPP L2 Peroxyacetyl Nitrate for Beijing* (Summary Product V1) [dataset]. Goddard Earth Sciences Data and Information Services Center (GES DISC). https://doi.org/10.5067/GBMBES47TUOI

Bowman, K. W. (2021c). *TROPESS CrIS-SNPP L2 Peroxyacetyl Nitrate for Delhi* (Standard Product V1) [dataset]. Goddard Earth Sciences Data and Information Services Center (GES DISC). https://doi.org/10.5067/NILL9KD1K78G

Bowman, K. W. (2021d). *TROPESS CrIS-SNPP L2 Peroxyacetyl Nitrate for Delhi* (Summary Product V1) [dataset]. Goddard Earth Sciences Data and Information Services Center (GES DISC). https://doi.org/10.5067/IHXG5JVO98VC

Bowman, K. W. (2021e). *TROPESS CrIS-SNPP L2 Peroxyacetyl Nitrate for Karachi* (Standard Product V1) [dataset]. Goddard Earth Sciences Data and Information Services Center (GES DISC). https://doi.org/10.5067/3AKYF8OS8DHK

Bowman, K. W. (2021f). *TROPESS CrIS-SNPP L2 Peroxyacetyl Nitrate for Karachi* (Summary Product V1) [dataset]. Goddard Earth Sciences Data and Information Services Center (GES DISC). https://doi.org/OHZ38O337SMK

Bowman, K. W. (2021g). *TROPESS CrIS-SNPP L2 Peroxyacetyl Nitrate for Lagos* (Standard Product, V1) [dataset]. Goddard Earth Sciences Data and Information Services Center (GES DISC). https://doi.org/10.5067/4UH0WF2HOHHB

Bowman, K. W. (2021h). *TROPESS CrIS-SNPP L2 Peroxyacetyl Nitrate for Lagos* (Summary Product V1) [dataset]. Goddard Earth Sciences Data and Information Services Center (GES DISC). https://doi.org/10.5067/G2FKY92PRSF5,

Bowman, K. W. (2021i). *TROPESS CrIS-SNPP L2 Peroxyacetyl Nitrate for Los Angeles* (Stanard Product V1) [dataset]. Goddard Earth Sciences Data and Information Services Center (GES DISC). https://doi.org/10.5067/0QPQFIXDET1X

Bowman, K. W. (2021j). *TROPESS CrIS-SNPP L2 Peroxyacetyl Nitrate for Los Angeles* (Summary Product V1) [dataset]. Goddard Earth Sciences Data and Information Services Center (GES DISC). https://doi.org/10.5067/H66DGC3ICJMQ

436 Bowman, K. W. (2021k). *TROPESS CrIS-SNPP L2 Peroxyacetyl Nitrate for Mexico City*
437 (Standard Product V1) [dataset]. Goddard Earth Sciences Data and Information Services
438 Center (GES DISC). https://doi.org/10.5067/PECEC1AZ5R1J
439 Bowman, K. W. (2021l). *TROPESS CrIS-SNPP L2 Peroxyacetyl Nitrate for Mexico City*
440 (Summary Product V1) [dataset]. Goddard Earth Sciences Data and Information Services
441 Center (GES DISC). https://doi.org/10.5067/YTO4AV07QQOW
442 Bowman, K. W. (2021m). *TROPESS CrIS-SNPP L2 Peroxyacetyl Nitrate for São Paulo*
443 (Standard Product V1) [dataset]. Goddard Earth Sciences Data and Information Services
444 Center (GES DISC). https://doi.org/10.5067/SQVOPBQTHU10
445 Bowman, K. W. (2021n). *TROPESS CrIS-SNPP L2 Peroxyacetyl Nitrate for São Paulo*
446 (Summary Product V1) [dataset]. Goddard Earth Sciences Data and Information Services
447 Center (GES DISC). https://doi.org/10.5067/AA26EWZUNMDK
448 Bowman, K. W. (2021o). *TROPESS CrIS-SNPP L2 Peroxyacetyl Nitrate for Tokyo* (Standard
449 Product V1) [dataset]. Goddard Earth Sciences Data and Information Services Center
450 (GES DISC). https://doi.org/10.5067/4UH0WF2HOHHB
451 Bowman, K. W. (2021p). *TROPESS CrIS-SNPP L2 Peroxyacetyl Nitrate for Tokyo* (Summary
452 Product V1) [dataset]. Goddard Earth Sciences Data and Information Services Center
453 (GES DISC). https://doi.org/10.5067/RAD13QSZ61JY
454 Brice, K. A., Bottenheim, J. W., Anlauf, K. G., & Wiebe, H. A. (1988). Long-term
455 measurements of atmospheric peroxyacetylnitrate (PAN) at rural sites in Ontario and
456 Nova Scotia; seasonal variations and long-range transport. *Tellus B*, *40B*(5), 408–425.
457 https://doi.org/10.1111/j.1600-0889.1988.tb00113.x

458 Cady-Pereira, K. E., Payne, V. H., Neu, J. L., Bowman, K. W., Miyazaki, K., Marais, E. A.,
459 Kulawik, S., Tzompa-Sosa, Z. A., & Hegarty, J. D. (2017). Seasonal and spatial changes
460 in trace gases over megacities from Aura TES observations: Two case studies.
461 *Atmospheric Chemistry and Physics*, *17*(15), 9379–9398. https://doi.org/10.5194/acp-17-
462 9379-2017
463 Chinazzi, M., Davis, J. T., Ajelli, M., Gioannini, C., Litvinova, M., Merler, S., Pastore y Piontti,
464 A., Mu, K., Rossi, L., Sun, K., Viboud, C., Xiong, X., Yu, H., Halloran, M. E., Longini,
465 I. M., & Vespignani, A. (2020). The effect of travel restrictions on the spread of the 2019
466 novel coronavirus (COVID-19) outbreak. *Science*, *368*(6489), 395–400.
467 https://doi.org/10.1126/science.aba9757
468 Clarisse, L., R'Honi, Y., Coheur, P.-F., Hurtmans, D., & Clerbaux, C. (2011). Thermal infrared
469 nadir observations of 24 atmospheric gases: TRACE GAS OBSERVATIONS FROM
470 IASI. *Geophysical Research Letters*, *38*(10), n/a-n/a.
471 https://doi.org/10.1029/2011GL047271
472 Coggon, M. M., Gkatzelis, G. I., McDonald, B. C., Gilman, J. B., Schwantes, R. H., Abuhassan,
473 N., Aikin, K. C., Arend, M. F., Berkoff, T. A., Brown, S. S., Campos, T. L., Dickerson,
474 R. R., Gronoff, G., Hurley, J. F., Isaacman-VanWertz, G., Koss, A. R., Li, M., McKeen,
475 S. A., Moshary, F., … Warneke, C. (2021). Volatile chemical product emissions enhance
476 ozone and modulate urban chemistry. *Proceedings of the National Academy of Sciences*,
477 *118*(32), e2026653118. https://doi.org/10.1073/pnas.2026653118
478 Connerton, P., Vicente de Assunção, J., Maura de Miranda, R., Dorothée Slovic, A., José Pérez-
479 Martínez, P., & Ribeiro, H. (2020). Air Quality during COVID-19 in Four Megacities:

480 Lessons and Challenges for Public Health. *International Journal of Environmental*
481 *Research and Public Health*, *17*(14), 5067. https://doi.org/10.3390/ijerph17145067
482 Damiani, A., Irie, H., Belikov, D. A., Kaizuka, S., Hoque, H. M. S., & Cordero, R. R. (2022).
483 Peculiar COVID-19 effects in the Greater Tokyo Area revealed by spatiotemporal
484 variabilities of tropospheric gases and light-absorbing aerosols. *Atmospheric Chemistry*
485 *and Physics*, *22*(18), 12705–12726. https://doi.org/10.5194/acp-22-12705-2022
486 De Smedt, I., Müller, J.-F., Stavrakou, T., van der A, R., Eskes, H., & Van Roozendael, M.
487 (2008). Twelve years of global observations of formaldehyde in the troposphere using
488 GOME and SCIAMACHY sensors. *Atmospheric Chemistry and Physics*, *8*(16), 4947–
489 4963. https://doi.org/10.5194/acp-8-4947-2008
490 De Smedt, I., Yu, H., Richter, A., Beirle, S., Eskes, H., Boersma, F., Van Roozendael, M., van
491 Geffen, J. H. G. M., Lorente, A., & Peters, E. (2017). *QA4ECV HCHO tropospheric*
492 *column data from OMI (Version 1.1) [L3 Monthly Means]*. Royal Belgian Institute for
493 Space Aeronomy. http://doi.org/10.18758/71021031
494 Feng, X., Li, Q., Zhu, Y., Hou, J., Jin, L., & Wang, J. (2015). Artificial neural networks
495 forecasting of PM2.5 pollution using air mass trajectory based geographic model and
496 wavelet transformation. *Atmospheric Environment*, *107*, 118–128.
497 https://doi.org/10.1016/j.atmosenv.2015.02.030
498 Fischer, E. V., Jacob, D. J., Yantosca, R. M., Sulprizio, M. P., Millet, D. B., Mao, J., Paulot, F.,
499 Singh, H. B., Roiger, A., Ries, L., Talbot, R. W., Dzepina, K., & Pandey Deolal, S.
500 (2014). Atmospheric peroxyacetyl nitrate (PAN): A global budget and source attribution.
501 *Atmospheric Chemistry and Physics*, *14*(5), 2679–2698. https://doi.org/10.5194/acp-14-
502 2679-2014

503 Fischer, E. V., Zhu, L., Payne, V. H., Worden, J. R., Jiang, Z., Kulawik, S. S., Brey, S.,
504 Hecobian, A., Gombos, D., Cady-Pereira, K., & Flocke, F. (2018). Using TES retrievals
505 to investigate PAN in North American biomass burning plumes. *Atmospheric Chemistry*
506 *and Physics*, *18*(8), 5639–5653. https://doi.org/10.5194/acp-18-5639-2018
507 Franco, B., Clarisse, L., Stavrakou, T., Müller, J. -F, Van Damme, M., Whitburn, S., Hadji-
508 Lazaro, J., Hurtmans, D., Taraborrelli, D., Clerbaux, C., & Coheur, P. -F. (2018). A
509 General Framework for Global Retrievals of Trace Gases From IASI: Application to
510 Methanol, Formic Acid, and PAN. *Journal of Geophysical Research: Atmospheres*,
511 *123*(24). https://doi.org/10.1029/2018JD029633
512 Fu, D., Bowman, K. W., Worden, H. M., Natraj, V., Worden, J. R., Yu, S., Veefkind, P., Aben,
513 I., Landgraf, J., Strow, L., & Han, Y. (2016). High-resolution tropospheric carbon
514 monoxide profiles retrieved from CrIS and TROPOMI. *Atmospheric Measurement*
515 *Techniques*, *9*(6), 2567–2579. https://doi.org/10.5194/amt-9-2567-2016
516 Gaffney, J. S., Marley, N. A., & Prestbo, E. W. (1989). Peroxyacyl Nitrates (PANs): Their
517 Physical and Chemical Properties. In O. Hutzinger (Ed.), *Air Pollution: Vol. 4 / 4B* (pp.
518 1–38). Springer Berlin Heidelberg. https://doi.org/10.1007/978-3-540-46113-5_1
519 Global Modeling and Assimilation Office (GMAO). (2015). *MERRA-2 tavgM_2d_slv_Nx:*
520 *2d,Monthly mean,Time-Averaged,Single-Level,Assimilation,Single-Level Diagnostics*
521 *V5.12.4*. Greenbelt, MD, USA, Goddard Earth Sciences Data and Information Services
522 Center (GES DISC). 10.5067/AP1B0BA5PD2K
523 Graedel, T. E., Bates, T. S., Bouwman, A. F., Cunnold, D., Dignon, J., Fung, I., Jacob, D. J.,
524 Lamb, B. K., Logan, J. A., Marland, G., Middleton, P., Pacyna, J. M., Placet, M., &

525 Veldt, C. (1993). A compilation of inventories of emissions to the atmosphere. *Global*
526 *Biogeochemical Cycles*, *7*(1), 1–26. https://doi.org/10.1029/92GB02793
527 Gurjar, B. R., Ravindra, K., & Nagpure, A. S. (2016). Air pollution trends over Indian megacities
528 and their local-to-global implications. *Atmospheric Environment*, *142*, 475–495.
529 https://doi.org/10.1016/j.atmosenv.2016.06.030
530 Honrath, R. E., Hamlin, A. J., & Merrill, J. T. (1996). Transport of ozone precursors from the
531 Arctic troposphere to the North Atlantic region. *Journal of Geophysical Research*,
532 *101*(D22), 29335–29351. https://doi.org/10.1029/95JD02673
533 Ito, A., Wakamatsu, S., Morikawa, T., & Kobayashi, S. (2021). 30 Years of Air Quality Trends
534 in Japan. *Atmosphere*, *12*(8), 1072. https://doi.org/10.3390/atmos12081072
535 Janssens-Maenhout, G., Crippa, M., Guizzardi, D., Dentener, F., Muntean, M., Pouliot, G.,
536 Keating, T., Zhang, Q., Kurokawa, J., Wankmüller, R., Denier van der Gon, H., Kuenen,
537 J. J. P., Klimont, Z., Frost, G., Darras, S., Koffi, B., & Li, M. (2015). HTAP_v2.2: A
538 mosaic of regional and global emission grid maps for 2008 and 2010 to study
539 hemispheric transport of air pollution. *Atmospheric Chemistry and Physics*, *15*(19),
540 11411–11432. https://doi.org/10.5194/acp-15-11411-2015
541 Jiang, Z., Worden, J. R., Payne, V. H., Zhu, L., Fischer, E., Walker, T., & Jones, D. B. A. (2016).
542 Ozone export from East Asia: The role of PAN. *Journal of Geophysical Research:*
543 *Atmospheres*, *121*(11), 6555–6563. https://doi.org/10.1002/2016JD024952
544 Jin, X., Fiore, A. M., Murray, L. T., Valin, L. C., Lamsal, L. N., Duncan, B., Folkert Boersma,
545 K., De Smedt, I., Abad, G. G., Chance, K., & Tonnesen, G. S. (2017). Evaluating a
546 Space-Based Indicator of Surface Ozone-NO_x-VOC Sensitivity Over Midlatitude
547 Source Regions and Application to Decadal Trends: Space-Based Indicator of O_3

548 Sensitivity. *Journal of Geophysical Research: Atmospheres*, *122*(19), 10,439-10,461.
549 https://doi.org/10.1002/2017JD026720
550 Juncosa Calahorrano, J. F., Payne, V. H., Kulawik, S., Ford, B., Flocke, F., Campos, T., &
551 Fischer, E. V. (2021). Evolution of Acyl Peroxynitrates (PANs) in Wildfire Smoke
552 Plumes Detected by the Cross-Track Infrared Sounder (CrIS) Over the Western U.S.
553 During Summer 2018. *Geophysical Research Letters*, *48*(23).
554 https://doi.org/10.1029/2021GL093405
555 Langford, A. O., Senff, C. J., Alvarez, R. J., Banta, R. M., & Hardesty, R. M. (2010). Long-
556 range transport of ozone from the Los Angeles Basin: A case study: LONG-RANGE
557 TRANSPORT OF OZONE. *Geophysical Research Letters*, *37*(6), n/a-n/a.
558 https://doi.org/10.1029/2010GL042507
559 Le, T., Wang, Y., Liu, L., Yang, J., Yung, Y. L., Li, G., & Seinfeld, J. H. (2020). Unexpected air
560 pollution with marked emission reductions during the COVID-19 outbreak in China.
561 *Science*, *369*(6504), 702–706. https://doi.org/10.1126/science.abb7431
562 Lee, H.-J., Chang, L.-S., Jaffe, D. A., Bak, J., Liu, X., Abad, G. G., Jo, H.-Y., Jo, Y.-J., Lee, J.-
563 B., & Kim, C.-H. (2021). Ozone Continues to Increase in East Asia Despite Decreasing
564 NO2: Causes and Abatements. *Remote Sensing*, *13*(11), 2177.
565 https://doi.org/10.3390/rs13112177
566 Li, K., Jacob, D. J., Liao, H., Qiu, Y., Shen, L., Zhai, S., Bates, K. H., Sulprizio, M. P., Song, S.,
567 Lu, X., Zhang, Q., Zheng, B., Zhang, Y., Zhang, J., Lee, H. C., & Kuk, S. K. (2021).
568 Ozone pollution in the North China Plain spreading into the late-winter haze season.
569 *Proceedings of the National Academy of Sciences*, *118*(10), e2015797118.
570 https://doi.org/10.1073/pnas.2015797118

571 Liang, Y., Sengupta, D., Campmier, M. J., Lunderberg, D. M., Apte, J. S., & Goldstein, A. H.
572 (2021). Wildfire smoke impacts on indoor air quality assessed using crowdsourced data
573 in California. *Proceedings of the National Academy of Sciences*, *118*(36), e2106478118.
574 https://doi.org/10.1073/pnas.2106478118
575 Liu, T., Chen, G., Chen, J., Xu, L., Li, M., Hong, Y., Chen, Y., Ji, X., Yang, C., Chen, Y.,
576 Huang, W., Huang, Q., & Wang, H. (2022). Seasonal characteristics of atmospheric
577 peroxyacetyl nitrate (PAN) in a coastal city of Southeast China: Explanatory factors and
578 photochemical effects. *Atmospheric Chemistry and Physics*, *22*(7), 4339–4353.
579 https://doi.org/10.5194/acp-22-4339-2022
580 Liu, Z., Ciais, P., Deng, Z., Lei, R., Davis, S. J., Feng, S., Zheng, B., Cui, D., Dou, X., He, P.,
581 Zhu, B., Lu, C., Ke, P., Sun, T., Yue, X., Wang, Y., Lei, Y., Zhou, H., Cai, Z., …
582 Schellnhuber, H. J. (n.d.). *Near-real-time data captured record decline in global CO2*
583 *emissions due to COVID-19*. 45.
584 Liu, Z., Wang, Y., Gu, D., Zhao, C., Huey, L. G., Stickel, R., Liao, J., Shao, M., Zhu, T., Zeng,
585 L., Liu, S.-C., Chang, C.-C., Amoroso, A., & Costabile, F. (2010). Evidence of Reactive
586 Aromatics As a Major Source of Peroxy Acetyl Nitrate over China. *Environmental*
587 *Science & Technology*, *44*(18), 7017–7022. https://doi.org/10.1021/es1007966
588 Martin, R. V., Fiore, A. M., & Van Donkelaar, A. (2004). Space-based diagnosis of surface
589 ozone sensitivity to anthropogenic emissions: SURFACE OZONE SENSITIVITY TO
590 EMISSIONS. *Geophysical Research Letters*, *31*(6), n/a-n/a.
591 https://doi.org/10.1029/2004GL019416
592 Mena-Carrasco, M., Carmichael, G. R., Campbell, J. E., Zimmerman, D., Tang, Y., Adhikary,
593 B., D'allura, A., Molina, L. T., Zavala, M., Garcıa, A., Flocke, F., Campos, T.,

Weinheimer, A. J., Shetter, R., Apel, E., Montzka, D. D., Knapp, D. J., & Zheng, W. (2009). Assessing the regional impacts of Mexico City emissions on air quality and chemistry. *Atmos. Chem. Phys.*, 13.

Miyazaki, K., Bowman, K., Sekiya, T., Eskes, H., Boersma, F., Worden, H., Livesey, N., Payne, V. H., Sudo, K., Kanaya, Y., Takigawa, M., & Ogochi, K. (2020). Updated tropospheric chemistry reanalysis and emission estimates, TCR-2, for 2005–2018. *Earth System Science Data*, *12*(3), 2223–2259. https://doi.org/10.5194/essd-12-2223-2020

Miyazaki, K., Bowman, K., Sekiya, T., Jiang, Z., Chen, X., Eskes, H., Ru, M., Zhang, Y., & Shindell, D. (2020). Air Quality Response in China Linked to the 2019 Novel Coronavirus (COVID-19) Lockdown. *Geophysical Research Letters*, *47*(19). https://doi.org/10.1029/2020GL089252

Miyazaki, K., Bowman, K., Sekiya, T., Takigawa, M., Neu, J. L., Sudo, K., Osterman, G., & Eskes, H. (2021). Global tropospheric ozone responses to reduced NOx emissions linked to the COVID-19 worldwide lockdowns. *SCIENCE ADVANCES*, 15.

Miyazaki, K., Eskes, H., Sudo, K., Boersma, K. F., Bowman, K., & Kanaya, Y. (2017). Decadal changes in global surface NO2; emissions from multi-constituent satellite data assimilation. *Atmospheric Chemistry and Physics*, *17*(2), 807–837. https://doi.org/10.5194/acp-17-807-2017

Nussbaumer, C. M., & Cohen, R. C. (2020). The Role of Temperature and NO_x in Ozone Trends in the Los Angeles Basin. *Environmental Science & Technology*, *54*(24), 15652–15659. https://doi.org/10.1021/acs.est.0c04910

Odekanle, E. L., Fakinle, B. S., Odejobi, O. J., Akangbe, O. E., Sonibare, J. A., Akeredolu, F. A., & Oladoja, O. M. (2022). COVID-19 induced restriction in developing countries and its

impacts on pollution load: Case study of Lagos mega city. *Heliyon*, *8*(8), e10402. https://doi.org/10.1016/j.heliyon.2022.e10402

Payne, V. H., Alvarado, M. J., Cady-Pereira, K. E., Worden, J. R., Kulawik, S. S., & Fischer, E. V. (2014). Satellite observations of peroxyacetyl nitrate from the Aura Tropospheric Emission Spectrometer. *Atmospheric Measurement Techniques*, *7*(11), 3737–3749. https://doi.org/10.5194/amt-7-3737-2014

Payne, V. H., Fischer, E. V., Worden, J. R., Jiang, Z., Zhu, L., Kurosu, T. P., & Kulawik, S. S. (2017). Spatial variability in tropospheric peroxyacetyl nitrate in the tropics from infrared satellite observations in 2005 and 2006. *Atmospheric Chemistry and Physics*, *17*(10), 6341–6351. https://doi.org/10.5194/acp-17-6341-2017

Payne, V. H., Kulawik, S. S., Fischer, E. V., Brewer, J. F., Huey, L. G., Miyazaki, K., Worden, J. R., Bowman, K. W., Hintsa, E. J., Moore, F., Elkins, J. W., & Juncosa Calahorrano, J. (2022). *Satellite measurements of peroxyacetyl nitrate from the Cross-Track Infrared Sounder: Comparison with ATom aircraft measurements*. Gases/Remote Sensing/Validation and Intercomparisons. https://doi.org/10.5194/amt-15-3497-2022

Penkett, S. A., & Brice, K. A. (1986). The spring maximum in photo-oxidants in the Northern Hemisphere troposphere. *Nature*, *319*(6055), 655–657. https://doi.org/10.1038/319655a0

Peralta, O., Ortínez-Alvarez, A., Torres-Jardón, R., Suárez-Lastra, M., Castro, T., & Ruíz-Suárez, L. G. (2021). Ozone over Mexico City during the COVID-19 pandemic. *Science of The Total Environment*, *761*, 143183. https://doi.org/10.1016/j.scitotenv.2020.143183

Pollack, I. B., Ryerson, T. B., Trainer, M., Neuman, J. A., Roberts, J. M., & Parrish, D. D. (2013). Trends in ozone, its precursors, and related secondary oxidation products in Los Angeles, California: A synthesis of measurements from 1960 to 2010: OZONE TRENDS

IN LA FROM 1960 TO 2010. *Journal of Geophysical Research: Atmospheres*, *118*(11), 5893–5911. https://doi.org/10.1002/jgrd.50472

Qiu, Y., Ma, Z., & Li, K. (2019). A modeling study of the peroxyacetyl nitrate (PAN) during a wintertime haze event in Beijing, China. *Science of The Total Environment*, *650*, 1944–1953. https://doi.org/10.1016/j.scitotenv.2018.09.253

Qiu, Y., Ma, Z., Li, K., Lin, W., Tang, Y., Dong, F., & Liao, H. (2020). Markedly Enhanced Levels of Peroxyacetyl Nitrate (PAN) During COVID-19 in Beijing. *Geophysical Research Letters*, *47*(19). https://doi.org/10.1029/2020GL089623

Randerson, J., van der verf, G., Gilglio, L., Collatz, G., & Kasibhatla, P. (2018). Global Fire Emissions Database, Version 4, (GFEDv4), ORNL DAAC. *Oak Ridge, Tennessee, USA*.

Rappenglück, B., Melas, D., & Fabian, P. (2003). Evidence of the impact of urban plumes on remote sites in the Eastern Mediterranean. *Atmospheric Environment*, *37*(13), 1853–1864. https://doi.org/10.1016/S1352-2310(03)00065-7

Roberts, J. M. (2007). PAN and Related Compounds. In R. Koppmann (Ed.), *Volatile Organic Compounds in the Atmosphere* (pp. 221–268). Blackwell Publishing Ltd. https://doi.org/10.1002/9780470988657.ch6

Saxena, P., Sonwani, S., Srivastava, A., Jain, M., Srivastava, A., Bharti, A., Rangra, D., Mongia, N., Tejan, S., & Bhardwaj, S. (2021). Impact of crop residue burning in Haryana on the air quality of Delhi, India. *Heliyon*, *7*(5), e06973. https://doi.org/10.1016/j.heliyon.2021.e06973

Schroeder, J. R., Cai, C., Xu, J., Ridley, D., Lu, J., Bui, N., Yan, F., & Avise, J. (2022). Changing ozone sensitivity in the South Coast Air Basin during the COVID-19 period.

Atmospheric Chemistry and Physics, *22*(19), 12985–13000. https://doi.org/10.5194/acp-22-12985-2022

Sharma, S., Zhang, M., Anshika, Gao, J., Zhang, H., & Kota, S. H. (2020). Effect of restricted emissions during COVID-19 on air quality in India. *Science of The Total Environment*, *728*, 138878. https://doi.org/10.1016/j.scitotenv.2020.138878

Shen, L., Jacob, D. J., Zhu, L., Zhang, Q., Zheng, B., Sulprizio, M. P., Li, K., De Smedt, I., González Abad, G., Cao, H., Fu, T., & Liao, H. (2019). The 2005–2016 Trends of Formaldehyde Columns Over China Observed by Satellites: Increasing Anthropogenic Emissions of Volatile Organic Compounds and Decreasing Agricultural Fire Emissions. *Geophysical Research Letters*, *46*(8), 4468–4475. https://doi.org/10.1029/2019GL082172

Shi, X., & Brasseur, G. P. (2020). The Response in Air Quality to the Reduction of Chinese Economic Activities During the COVID-19 Outbreak. *Geophysical Research Letters*, *47*(11). https://doi.org/10.1029/2020GL088070

Shogrin, M. J. (2023). *CrIS PANs megacity dataset for São Paulo and Lagos* [..Csv]. Dryad. https://doi.org/10.5061/dryad.wpzgmsbtk

Shogrin, M. J., Payne, V. H., Kulawik, S. S., Miyazaki, K., & Fischer, E. V. (2023). Measurement report: Spatiotemporal variability of peroxy acyl nitrates (PANs) over Mexico City from TES and CrIS satellite measurements. *Atmospheric Chemistry and Physics*, *23*(4), 2667–2682. https://doi.org/10.5194/acp-23-2667-2023

Sicard, P., De Marco, A., Agathokleous, E., Feng, Z., Xu, X., Paoletti, E., Rodriguez, J. J. D., & Calatayud, V. (2020). Amplified ozone pollution in cities during the COVID-19 lockdown. *Science of The Total Environment*, *735*, 139542. https://doi.org/10.1016/j.scitotenv.2020.139542

685 Sillman, S., & West, J. J. (2009). Reactive nitrogen in Mexico City and its relation to ozone-
686 precursor sensitivity: Results from photochemical models. *Atmos. Chem. Phys.*, 13.
687 Singh, H. B., & Hanst, P. L. (1981). Peroxyacetyl nitrate (PAN) in the unpolluted atmosphere:
688 An important reservoir for nitrogen oxides. *Geophysical Research Letters*, *8*(8), 941–944.
689 https://doi.org/10.1029/GL008i008p00941
690 Singh, H. B., Salas, L. J., & Viezee, W. (1986). Global distribution of peroxyacetyl nitrate.
691 *Nature*, *321*(6070), 588–591. https://doi.org/10.1038/321588a0
692 Souri, A. H., Johnson, M. S., Wolfe, G. M., Crawford, J. H., Fried, A., Wisthaler, A., Brune, W.
693 H., Blake, D. R., Weinheimer, A. J., Verhoelst, T., Compernolle, S., Pinardi, G.,
694 Vigouroux, C., Langerock, B., Choi, S., Lamsal, L., Zhu, L., Sun, S., Cohen, R. C., …
695 Chance, K. (2023). Characterization of errors in satellite-based HCHO ⁄ NO $_2$
696 tropospheric column ratios with respect to chemistry, column-to-PBL translation, spatial
697 representation, and retrieval uncertainties. *Atmospheric Chemistry and Physics*, *23*(3),
698 1963–1986. https://doi.org/10.5194/acp-23-1963-2023
699 Souri, A. H., Nowlan, C. R., Wolfe, G. M., Lamsal, L. N., Chan Miller, C. E., Abad, G. G., Janz,
700 S. J., Fried, A., Blake, D. R., Weinheimer, A. J., Diskin, G. S., Liu, X., & Chance, K.
701 (2020). Revisiting the effectiveness of HCHO/NO2 ratios for inferring ozone sensitivity
702 to its precursors using high resolution airborne remote sensing observations in a high
703 ozone episode during the KORUS-AQ campaign. *Atmospheric Environment*, *224*,
704 117341. https://doi.org/10.1016/j.atmosenv.2020.117341
705 Stavrakou, T., Müller, J.-F., Bauwens, M., Doumbia, T., Elguindi, N., Darras, S., Granier, C.,
706 Smedt, I. D., Lerot, C., Van Roozendael, M., Franco, B., Clarisse, L., Clerbaux, C.,
707 Coheur, P.-F., Liu, Y., Wang, T., Shi, X., Gaubert, B., Tilmes, S., & Brasseur, G. (2021).

Atmospheric Impacts of COVID-19 on NOx and VOC Levels over China Based on TROPOMI and IASI Satellite Data and Modeling. *Atmosphere*, *12*(8), 946. https://doi.org/10.3390/atmos12080946

Steiner, A. L., Davis, A. J., Sillman, S., Owen, R. C., Michalak, A. M., & Fiore, A. M. (2010). Observed suppression of ozone formation at extremely high temperatures due to chemical and biophysical feedbacks. *Proceedings of the National Academy of Sciences*, *107*(46), 19685–19690. https://doi.org/10.1073/pnas.1008336107

Venter, Z. S., Aunan, K., Chowdhury, S., & Lelieveld, J. (2020). COVID-19 lockdowns cause global air pollution declines. *Proceedings of the National Academy of Sciences*, *117*(32), 18984–18990. https://doi.org/10.1073/pnas.2006853117

Wang, L., Jin, X., Wang, Q., Mao, H., Liu, Q., Weng, G., & Wang, Y. (2020). Spatial and temporal variability of open biomass burning in Northeast China from 2003 to 2017. *Atmospheric and Oceanic Science Letters*, *13*(3), 240–247. https://doi.org/10.1080/16742834.2020.1742574

Wang, Q., & Li, S. (2021). Nonlinear impact of COVID-19 on pollutions – Evidence from Wuhan, New York, Milan, Madrid, Bandra, London, Tokyo and Mexico City. *Sustainable Cities and Society*, *65*, 102629. https://doi.org/10.1016/j.scs.2020.102629

Warneke, C., de Gouw, J. A., Edwards, P. M., Holloway, J. S., Gilman, J. B., Kuster, W. C., Graus, M., Atlas, E., Blake, D., Gentner, D. R., Goldstein, A. H., Harley, R. A., Alvarez, S., Rappenglueck, B., Trainer, M., & Parrish, D. D. (2013). Photochemical aging of volatile organic compounds in the Los Angeles basin: Weekday-weekend effect: VOC WEEKDAY-WEEKEND EFFECT. *Journal of Geophysical Research: Atmospheres*, *118*(10), 5018–5028. https://doi.org/10.1002/jgrd.50423

731 WHO. (2020). *Coronavirus disease 2019 (COVID-19): Situation Report – 43*.
732 www.who.int/docs/default-source/coronaviruse/situation-reports/20200303-sitrep-43-
733 covid-19.pdf?sfvrsn=2c21c09c_2.
734 Worden, H. M., Francis, G. L., Kulawik, S. S., Bowman, K. W., Cady-Pereira, K., Fu, D.,
735 Hegarty, J. D., Kantchev, V., Luo, M., Payne, V. H., Worden, J. R., Commane, R., &
736 McKain, K. (2022). *TROPESS/CrIS carbon monoxide profile validation with NOAA*
737 *GML and ATom in situ aircraft observations* [Preprint]. Gases/Remote
738 Sensing/Validation and Intercomparisons. https://doi.org/10.5194/amt-2022-128
739 Yin, L., Du, P., Zhang, M., Liu, M., Xu, T., & Song, Y. (2019). Estimation of emissions from
740 biomass burning in China (2003–2017) based on MODIS fire radiative energy data.
741 *Biogeosciences*, *16*(7), 1629–1640. https://doi.org/10.5194/bg-16-1629-2019
742 Yoshitomi, M., Wild, O., & Akimoto, H. (2011). *Contributions of regional and intercontinental*
743 *transport to surface ozone in Tokyo* [Preprint]. Gases/Atmospheric
744 Modelling/Troposphere/Chemistry (chemical composition and reactions).
745 https://doi.org/10.5194/acpd-11-10403-2011
746 Zhang, B., Zhao, B., Zuo, P., Huang, Z., & Zhang, J. (2017). Ambient peroxyacyl nitrate
747 concentration and regional transportation in Beijing. *Atmospheric Environment*, *166*,
748 543–550. https://doi.org/10.1016/j.atmosenv.2017.07.053
749 Zhang, B., Zhao, X., & Zhang, J. (2019). Characteristics of peroxyacetyl nitrate pollution during
750 a 2015 winter haze episode in Beijing. *Environmental Pollution*, *244*, 379–387.
751 https://doi.org/10.1016/j.envpol.2018.10.078
752 Zhang, G., Mu, Y., Zhou, L., Zhang, C., Zhang, Y., Liu, J., Fang, S., & Yao, B. (2015a).
753 Summertime distributions of peroxyacetyl nitrate (PAN) and peroxypropionyl nitrate

(PPN) in Beijing: Understanding the sources and major sink of PAN. *Atmospheric Environment*, *103*, 289–296. https://doi.org/10.1016/j.atmosenv.2014.12.035

Zhang, G., Mu, Y., Zhou, L., Zhang, C., Zhang, Y., Liu, J., Fang, S., & Yao, B. (2015b). Summertime distributions of peroxyacetyl nitrate (PAN) and peroxypropionyl nitrate (PPN) in Beijing: Understanding the sources and major sink of PAN. *Atmospheric Environment*, *103*, 289–296. https://doi.org/10.1016/j.atmosenv.2014.12.035

Zhang, G., Xia, L., Zang, K., Xu, W., Zhang, F., Liang, L., Yao, B., Lin, W., & Mu, Y. (2020). The abundance and inter-relationship of atmospheric peroxyacetyl nitrate (PAN), peroxypropionyl nitrate (PPN), O3, and NOy during the wintertime in Beijing, China. *Science of The Total Environment*, *718*, 137388. https://doi.org/10.1016/j.scitotenv.2020.137388

Zhang, J., Lim, Y.-H., Andersen, Z. J., Napolitano, G., Taghavi Shahri, S. M., So, R., Plucker, M., Danesh-Yazdi, M., Cole-Hunter, T., Therming Jørgensen, J., Liu, S., Bergmann, M., Jayant Mehta, A., H. Mortensen, L., Requia, W., Lange, T., Loft, S., Kuenzli, N., Schwartz, J., & Amini, H. (2022). Stringency of COVID-19 Containment Response Policies and Air Quality Changes: A Global Analysis across 1851 Cities. *Environmental Science & Technology*, *56*(17), 12086–12096. https://doi.org/10.1021/acs.est.2c04303

Zhao, Y., Xu, R., Xu, Z., Wang, L., & Wang, P. (2022). Temporal and Spatial Patterns of Biomass Burning Fire Counts and Carbon Emissions in the Beijing–Tianjin–Hebei (BTH) Region during 2003–2020 Based on GFED4. *Atmosphere*, *13*(3), 459. https://doi.org/10.3390/atmos13030459

Zhu, L., Fischer, E. V., Payne, V. H., Worden, J. R., & Jiang, Z. (2015). TES observations of the interannual variability of PAN over Northern Eurasia and the relationship to springtime

777 fires. *Geophysical Research Letters*, *42*(17), 7230–7237.
778 https://doi.org/10.1002/2015GL065328
779 Zhu, L., Payne, V. H., Walker, T. W., Worden, J. R., Jiang, Z., Kulawik, S. S., & Fischer, E. V.
780 (2017). PAN in the eastern Pacific free troposphere: A satellite view of the sources,
781 seasonality, interannual variability, and timeline for trend detection. *Journal of*
782 *Geophysical Research: Atmospheres*, *122*(6), 3614–3629.
783 https://doi.org/10.1002/2016JD025868
784